Benchmark calculation of n-^{3}H and p-^{3}He scattering

M. Viviani,[1] A. Deltuva,[2] R. Lazauskas,[3] J. Carbonell,[4] A. C. Fonseca,[2] A. Kievsky,[1] L.E. Marcucci,[1,5] and S. Rosati[1,5]

[1]*INFN-Pisa, I-56127 Pisa, Italy*

[2]*Centro de Física Nuclear da Universidade de Lisboa, P-1649-003 Lisboa, Portugal*

[3]*IPHC, IN2P3-CNRS/Université Louis Pasteur BP 28, F-67037 Strasbourg Cedex 2, France*

[4]*CEA-Saclay, IRFU/SPhN, F-91191 Gif-sur-Yvette, France*

[5]*Department of Physics, University of Pisa, I-56127 Pisa, Italy*

(Received 16 September 2011; published 28 November 2011)

The n-^{3}H and p-^{3}He elastic phase shifts below the trinucleon disintegration thresholds are calculated by solving the four-nucleon problem with three different realistic nucleon-nucleon interactions (the I-N3LO model by Entem and Machleidt, the Argonne v_{18} potential model, and a low-k model derived from the CD-Bonn potential). Three different methods—Alt-Grassberger-Sandhas, hyperspherical harmonics, and Faddeev-Yakubovsky—have been used and their respective results are compared. For both n-^{3}H and p-^{3}He we observe a rather good agreement between the three different theoretical methods. We also compare the theoretical predictions with the available experimental data, confirming the large underprediction of the p-^{3}He analyzing power.

DOI: 10.1103/PhysRevC.84.054010 PACS number(s): 21.45.−v, 21.30.−x, 24.70.+s, 25.10.+s

I. INTRODUCTION

The four-nucleon ($4N$) system has been object of intense studies in recent years. In first place, this system is particularly interesting as a "theoretical laboratory" to test the accuracy of our present knowledge of the nucleon-nucleon (NN) and three-nucleon ($3N$) interactions. In particular, the effects of the NN P waves and of the $3N$ force are believed to be larger than in the $A = 2$ or 3 systems. Moreover, it is the simplest system where the $3N$ interaction in channels of total isospin $T = 3/2$ can be studied. In second place, there is a number of reactions involving four nucleons which are of extreme importance for astrophysics, energy production, and studies of fundamental symmetries. As an example, reactions like $d + d \to {}^4\mathrm{He} + \gamma$ or $p + {}^3\mathrm{He} \to {}^4\mathrm{He} + \nu_e + e^+$ (the *hep* process) play important roles in solar models and in the theory of big-bang nucleosynthesis.

Nowadays, the $4N$ bound-state problem can be numerically solved with good accuracy. For example, in Ref. [1] the binding energies and other properties of the α-particle were studied using the AV8′ [2] NN interaction; several different techniques produced results in very close agreement with each other (at the level of less than 1%). More recently, the same agreement has also been obtained considering different realistic NN+$3N$ force models [3–6].

In recent years, there has also been a rapid advance in solving the $4N$ scattering problem with realistic Hamiltonians. Accurate calculations of four-body scattering observables have been achieved in the framework of the Alt-Grassberger-Sandhas (AGS) equations [7–11], solved in momentum space, where the long-range Coulomb interaction is treated using the screening and renormalization method [12,13]. Solutions of the Faddeev-Yakubovsky (FY) equations in configuration space [14–18] and the application of the hyperspherical harmonics (HH) expansion method [19] to the solution of this problem also have been reported [20,21].

In addition to these methods, the solution of the $4N$ scattering problem has been obtained also by using the resonating group model (RGM) method [22–25]. Calculations of scattering observables using the Green's function Monte Carlo method are also underway [26].

The $4N$ studies performed so far have evidenced several discrepancies between theoretical predictions and experimental data. Let us consider first n-^{3}H elastic scattering. Calculations based on NN interaction models disagree [5,7,20] rather sizeably with the measured total cross section [27], both at zero energy and in the "peak" region ($E_n \approx 3.5$ MeV). This observable is found to be very sensitive to the NN interaction model [7]. At low energy, the discrepancy is removed by including a $3N$ force fixed to reproduce the triton binding energy [14,20,23,28], but it remains in the peak region. The analysis of the differential cross section has shown similar discrepancies, but definitive conclusions are difficult to extract since the experimental errors are rather large.

In this respect, the p-^{3}He elastic scattering is more interesting since there exist several accurate measurements of both the unpolarized cross section [29–31] and the proton analyzing power A_{y0} [31–33]. The calculations performed so far (with a variety of NN and NN+$3N$ interactions) have shown a large discrepancy between theory and experiment for A_{y0} [8,17,31,33,34]. In addition, at the Triangle Universities Nuclear Laboratory (TUNL), there has been recently a new set of accurate measurements of other p-^{3}He observables (the ^{3}He analyzing power A_{0y} and some spin-correlation observables as A_{yy}, A_{xx}, A_{xz}, A_{zx}, and A_{zz}) at $E_p = 1.60$, 2.25, 4.05, and 5.54 MeV, which has allowed a phase-shift analysis (PSA) [35]. A preliminary comparison with these data was reported in Ref. [21].

In order to have definite answer about the ability of the different interaction models to reproduce the experimental data it is certainly of interest to establish the accuracy reached by the theoretical methods in the solution of the $A = 4$ scattering problem. In a previous benchmark, the results obtained by different groups working with different techniques were found to be at variance with each other [17]. Clearly, this situation should be clarified before questioning the ability of present

NN+3N force models to describe the experimental data beyond the binding energy of ^{4}He. This is the purpose of the present paper, in which we present low-energy n-^{3}H and p-^{3}He scattering results obtained by the three different groups, using independent methods to solve the four-body problem, i.e., the AGS equations, the variational HH expansion, and the FY equations.

The potentials used in this paper are the I-N3LO model by Entem and Machleidt [36], with cutoff $\Lambda = 500$ MeV, the Argonne v_{18} (AV18) potential model [37], and a low-k model derived from the CD-Bonn potential [38]. The I-N3LO potential has been derived using an effective-field-theory approach and the chiral perturbation theory up to next-to-next-to-next-to-leading order. The AV18 potential is a phenomenological potential having a rather strong repulsion at short interparticle distances. The low-k potentials have been obtained separating the Hilbert space into low- and high-momentum regions and using the renormalization group method [38] to integrate out the high-momentum components above a cutoff Λ. The low-k potential adopted in this work is obtained starting from the realistic CD-Bonn potential [39] and using a smooth cutoff $\Lambda = 2.5$ fm^{-1}. The cut of the high-momentum part is reflected in configuration space in an almost total absence of the repulsion at short interparticle distances. Note that the first and third models are nonlocal, while AV18 is local in configuration space. The three potentials reproduce equally well the np and pp data and are a representative set of the large variety of modern NN potential models. We note, finally, that I-N3LO and AV18 interactions, without the inclusion of a suitable 3N interaction model, largely underestimate the ^{4}He binding energy $B(^4\text{He})$. On the contrary, with the adopted low-k potential model we have $B(^4\text{He}) = 29.04$ MeV, slightly overestimating the experimental value of 28.30 MeV.

This article is organized as follows. In Sec. II, a brief description of the methods used for this benchmark is reported. In Sec. III, a comparison between the results obtained within the different schemes is shown. In Sec. IV, the theoretical calculations are compared with the available experimental data. The conclusions will be given in Sec. V.

II. METHODS

In order to solve the 4N scattering problem we employ the AGS equations, the HH method, and the FY equations. The various procedures are briefly described below.

The total kinetic energy, $T_{\text{c.m.}}$, in the center of mass (c.m.) and the nucleon kinetic energy, E_N ($N = p, n$), in the laboratory reference frame are given by

$$T_{\text{c.m.}} = \frac{q^2}{2\mu}, \quad E_N = \frac{4}{3} T_{\text{c.m.}}, \tag{1}$$

where $\mu = (3/4)M_N$ is the reduced mass of the 1+3 system, M_N is the nucleon mass, and q the magnitude of the relative momentum between the two clusters.

A. AGS equations

The AGS equations [40] are integral equations for the four-body transition operators. They are well-defined only with short-range potentials. Nevertheless, together with the screening and renormalization method [8,41], they can be applied also to the reactions involving charged particles. In the 4N system we use the isospin formalism and solve the symmetrized form of the AGS equations [7]. In this case there are only two distinct four-particle partitions, one of the 3+1 type and one of the 2+2 type. We choose those partitions to be (12,3)4 and (12)(34) and denote them in the following by $\alpha = 1$ and 2, respectively. The corresponding transition operators $\mathcal{U}_{\beta\alpha}$ for the initial states of the 3+1 type, as appropriate for the n-^{3}H and p-^{3}He scattering, obey the integral equations

$$\begin{aligned}\mathcal{U}_{11} &= -(G_0\,T\,G_0)^{-1} P_{34} - P_{34}\,U_1\,G_0\,T\,G_0\,\mathcal{U}_{11} \\ &\quad + U_2 G_0\,T\,G_0\,\mathcal{U}_{21}, \end{aligned} \tag{2}$$

$$\mathcal{U}_{21} = (G_0\,T\,G_0)^{-1}\,(1 - P_{34}) + (1 - P_{34}) U_1\,G_0\,T\,G_0\,\mathcal{U}_{11}. \tag{3}$$

Here $G_0 = (E + i\epsilon - H_0)^{-1}$ is the free resolvent, E being the energy of the 4N system and H_0 the free Hamiltonian, and P_{ij} is the permutation operator of particles i and j. The (short-range) two-nucleon potential V^s enters the AGS equations via the two-nucleon transition matrix $T = V^s + V^s G_0 T$ and the 3+1 and 2+2 subsystem transition operators

$$U_\alpha = P_\alpha G_0^{-1} + P_\alpha\,T G_0\,U_\alpha, \tag{4}$$

where $P_1 = P_{12}\,P_{23} + P_{13}\,P_{23}$ and $P_2 = P_{13}\,P_{24}$. The 3+1 elastic-scattering amplitudes are given by $\langle \mathbf{p}_f|\mathcal{T}|\mathbf{p}_i\rangle = 3\langle \Psi_1(\mathbf{p}_f)|\mathcal{U}_{11}|\Psi_1(\mathbf{p}_i)\rangle$, where the factor 3 results from the symmetrization and $|\Psi_\alpha(\mathbf{p}_j)\rangle$ are properly normalized initial/final channel state Faddeev components.

In order to include the Coulomb interaction V^C between the protons in the p-^{3}He scattering we use the screening and renormalization approach [8,41]. We add to the nuclear pp potential the screened Coulomb one $V^R(r) = V^C(r)\,\exp[-(r/R)^n]$. Thus, the AGS equations with $V^s + V^R$ are well defined but all transition operators and the resulting amplitudes depend on the screening radius R. The renormalization procedure in the $R \to \infty$ limit yields the full p-^{3}He transition amplitude

$$\begin{aligned}\langle \mathbf{p}_f|\mathcal{T}_{(C)}|\mathbf{p}_i\rangle &= \langle \mathbf{p}_f|t_C^{\text{c.m.}}|\mathbf{p}_i\rangle \\ &\quad + \lim_{R\to\infty} \langle \mathbf{p}_f|\big[\mathcal{T}_{(R)} - t_R^{\text{c.m.}}\big]|\mathbf{p}_i\rangle Z_R^{-1}, \end{aligned} \tag{5}$$

where $\langle \mathbf{p}_f|t_C^{\text{c.m.}}|\mathbf{p}_i\rangle$ and $\langle \mathbf{p}_f|t_R^{\text{c.m.}}|\mathbf{p}_i\rangle$ are the proper and screened Coulomb amplitudes between the center of mass of two charged clusters, respectively; the former is known analytically. The renormalization factor Z_R is defined in Ref. [8]. Thus, the long- and Coulomb-distorted short-range parts in the scattering amplitudes are isolated and their infinite R limit is calculated separately. The long-range part of the amplitude $\langle \mathbf{p}_f|t_R^{\text{c.m.}}|\mathbf{p}_i\rangle$ is of two-body nature and its $R \to \infty$ limit after renormalization is $\langle \mathbf{p}_f|t_C^{\text{c.m.}}|\mathbf{p}_i\rangle$. The Coulomb-distorted short-range part $[\mathcal{T}_{(R)} - t_R^{\text{c.m.}}]$ is calculated by solving the AGS equations for $V^s + V^R$ numerically at a finite R that is sufficiently large to get R-independent results after the renormalization. In other words, the $R \to \infty$ limit is reached

with sufficient accuracy at finite R. However, R must be considerably larger than the range of the nuclear interaction, thereby leading to a slower partial-wave convergence. The right choice of the screening, i.e., the exponent n, is essential in dealing with this difficulty. For a fast convergence with R we have to ensure that $V^R(r)$ approximates well $V^C(r)$ for $r < R$ and simultaneously vanishes smoothly but rapidly for $r > R$, providing a comparatively fast convergence of the partial-wave expansion. Using the optimal value $n = 4$ we obtain reasonably converged results with R ranging from 10 to 15 fm and including two-proton partial waves with orbital angular momentum up to 10. The R convergence is slower at lower energies; the worst cases are the S waves at $E_p = 2.25$ MeV where we estimate the accuracy of our phase shift results to be around 1%. In contrast, the n-^{3}H results are converged very well, considerably better than 0.2%, as demonstrated in Ref. [7] where also the details on the included partial waves can be found.

B. HH expansion

The wave function describing a n-^{3}H or p-^{3}He scattering state with total angular-momentum quantum numbers J, J_z; incoming relative orbital angular momentum L; and channel spin S ($S = 0, 1$) can be written as

$$\Psi_{1+3}^{LS,JJ_z} = \Psi_C^{LS,JJ_z} + \Psi_A^{LS,JJ_z}, \tag{6}$$

where the part Ψ_C^{LS,JJ_z} describes the system in the region where the particles are close to each other and their mutual interactions are strong. Hence, Ψ_C^{LS,JJ_z} vanishes in the limit of large intercluster distances. This part of the wave function is written as a linear expansion $\sum_\mu c_\mu^{LSJ}\mathcal{Y}_\mu$, where $\mathcal{Y}_\mu$ is a set of basis functions constructed in terms of the HH functions (for more details, see, for example, Ref. [19]).

The other part Ψ_A^{LS,JJ_z} describes the relative motion of the two clusters in the asymptotic regions, where the 1+3 interaction is negligible (except eventually for the long-range Coulomb interaction). In the asymptotic region the wave functions Ψ_{1+3}^{LS,JJ_z} reduces to Ψ_A^{LS,JJ_z}, which must, therefore, be the appropriate asymptotic solution of the Schrödinger equation. Let us consider, for example, the p-^{3}He case. Then, Ψ_A^{LS,JJ_z} can be decomposed as a linear combination of the following functions:

$$\Omega^{\pm}_{LS,JJ_z} = \sum_{l=1}^{4}\big[Y_L(\hat{\mathbf{y}}_l)\otimes[\phi_3(ijk)\otimes s_l]_S\big]_{JJ_z} \times\left[f_L(y_l)\frac{G_L(\eta,qy_l)}{qy_l}\pm \mathrm{i}\frac{F_L(\eta,qy_l)}{qy_l}\right], \tag{7}$$

where $\mathbf{y}_l$ is the distance between the proton (particle l) and ^{3}He (particles ijk), q is the magnitude of the relative momentum between the two clusters, s_l the spin state of particle l, and ϕ_3 is the ^{3}He wave function. Moreover, F_L and G_L are the regular and irregular Coulomb function, respectively, with $\eta = 2\mu e^2/q$. The function $f_L(y) = [1-\exp(-\beta y)]^{2L+1}$ in Eq. (7) has been introduced to regularize G_L at small y, and $f_L(y)\to 1$ as y is large, thus not affecting the asymptotic behavior of Ψ_{1+3}^{LS,JJ_z}. Note that for large values of qy_l,

$$f_L(y_l)G_L(\eta,qy_l)\pm \mathrm{i}F_L(\eta,qy_l)\to \exp[\pm\mathrm{i}(qy_l - L\pi/2 - \eta\ln(2qy_l)+\sigma_L)], \tag{8}$$

where σ_L is the Coulomb phase shift. Therefore, Ω^+_{LS,JJ_z} (Ω^-_{LS,JJ_z}) describe the asymptotic outgoing (ingoing) p-^{3}He relative motion. Finally,

$$\Psi_A^{LS,JJ_z} = \sum_{L'S'}\left[\delta_{LL'}\delta_{SS'}\Omega^-_{LS,JJ_z} - \mathcal{S}^{J\pi}_{LS,L'S'}\Omega^+_{L'S',JJ_z}\right], \tag{9}$$

where the parameters $\mathcal{S}^{J\pi}_{LS,L'S'}$ are the S-matrix elements which determine phase shifts and (for coupled channels) mixing parameters at the energy $T_{\mathrm{c.m.}}$. Of course, the sum over L' and S' is over all values compatible with the given J and parity π. In particular, the sum over L' is limited to include either even or odd values such that $(-1)^{L'} = (-)^L = \pi$.

The S-matrix elements $\mathcal{S}^{J\pi}_{LS,L'S'}$ and coefficients c_μ^{LSJ} occurring in the HH expansion of Ψ_C^{LS,JJ_z} are determined by making the functional

$$\left[\mathcal{S}^{J\pi}_{LS,L'S'}\right] = \mathcal{S}^{J\pi}_{LS,L'S'} - \left\langle\Psi_{1+3}^{L'S',JJ_z}|H-E|\Psi_{1+3}^{LS,JJ_z}\right\rangle \tag{10}$$

stationary with respect to variations in the $\mathcal{S}^{J\pi}_{LS,L'S'}$ and c_μ^{LSJ} (Kohn variational principle). In the above equation, $E = T_{\mathrm{c.m.}} - B(^3\mathrm{He})$ is the energy of the system, $B(^3\mathrm{He})$ being the ^{3}He binding energy. By applying this principle, a linear set of equations is obtained for $\mathcal{S}^{J\pi}_{LS,L'S'}$ and c_μ^{LSJ}. This linear system is solved using the Lanczos algorithm.

This method can be applied in either coordinate or momentum space and using either local or nonlocal potentials [19] (see also Ref. [42] for an application to the $A = 3$ scattering problem). The first step is a partial-wave decomposition of the asymptotic functions $\Omega^{\pm}_{LS,JJ_z}$, a task which can be rather time-consuming, in particular, for the $J^\pi = 2^-$ state. After this decomposition, the calculation of the matrix element in Eq. (10) is fast. The problem then reduces to the solution of the linear system, which is performed using an iterative method (however, this solution has to be repeated several times due to the necessity to extrapolate the results; see below).

The expansion of the scattering wave function in terms of the HH basis is, in principle, infinite, therefore, a truncation scheme is necessary. The HH functions are essentially characterized by the orbital angular-momentum quantum numbers ℓ_i, $i = 1, 3$, associated with the three Jacobi vectors, and the grand angular quantum number K (each HH function is a polynomial of degree K). The basis is truncated to include states with $\ell_1+\ell_2+\ell_3 \leqslant \ell_{\max}$ (with all possible recoupling between angular and spin states appropriate to the given J). Between these states, we retain only the HH functions with $K \leqslant K_{\max}$. In the calculation we have included only states with total isospin $T = 1$.

The numerical uncertainty comes from the numerical integrations needed to compute the matrix elements of the Hamiltonian and the truncation of the basis. It has been checked that the numerical uncertainty of the calculated phase shifts related to the numerical integration is small (around

0.1%). The NN interaction has been limited to act on two-body states with total angular momentum $j \leqslant j_{\max} = 8$ (at the considered energies, greater values of $j_{\max}$ are completely unnecessary). The largest uncertainty is, thus, related to the use of a finite basis. The convergence with $\ell_{\max}$ is rather fast and the value $\ell_{\max} = 6$ have been found to be sufficient. The main problem is related to the slow convergence of the results with $K_{\max}$. This problem can be partly overcome by performing calculations for increasing values of $K_{\max}$ and then using some extrapolation rule (see, for example, Ref. [31]) to get the "$K_{\max} \to \infty$" result. This procedure has an uncertainty which can be estimated. A detailed study of this problem will be published elsewhere [43]. The convergence of the quantities of interest in term of $K_{\max}$ is slower when NN potentials with a strong repulsion at short interparticle distance are used such as for the AV18 potential. In this case we have estimated the uncertainty to be of the order of 0.5% in the extrapolated phase shifts. This problem is less relevant for the I-N3LO and the low-k models. In these cases, the uncertainty has been estimated to be at most 0.3%.

C. FY equations in configuration space

In the late 1960s, Yakubovsky [44] has managed to generalize the three-body equations derived by Faddeev [45] to an arbitrary number of particles. These equations were primarily derived for a system of particles submitted to short-range pairwise potential V^s. Nevertheless, it becomes possible to include also repulsive Coulomb interaction if these, the so-called Faddeev-Yakubovsky equations, are formulated in configuration space. To this aim, we split the Coulomb potential V^C into two parts (short and long range), $V^C = V^{s.C} + V^{l.C}$. The splitting procedure is quite arbitrary, and one should only take care that the long-range part $V^{l.C}$ of the Coulomb potential approaches sufficiently fast the full Coulomb interaction V^C when any of interparticle distances becomes large. The simplest application of FY equations is the problem of four identical particles. They result into a set of two differential equations coupling the two so-called FY components, namely $K^4_{12,3}$ and H^{34}_{12}, and have the form

$$\left(E - H_0 - V^s_{12} - \sum_{i<j} V^{l.C}_{ij}\right) K^4_{12,3} = \left(V^s_{12} + V^{s.C}_{12}\right) P_1 \left[(1 + \varepsilon P_{34}) K^4_{12,3} + H^{34}_{12}\right], \quad (11)$$

$$\left(E - H_0 - V^s_{12} - \sum_{i<j} V^{l.C}_{ij}\right) H^{34}_{12} = \left(V^s_{12} + V^{s.C}_{12}\right) P_2 \left[(1 + \varepsilon P_{34}) K^4_{12,3} + H^{34}_{12}\right], \quad (12)$$

where P_1, P_2, and P_{34} are the particle permutation operators, equivalent to those described in subsection II A, and $\varepsilon = \pm 1$ is a phase accounting for the Pauli principle between two identical particles ($\varepsilon = +1$ for bosons and $\varepsilon = -1$ for fermions).

Each FY component $F = (K, H)$ is considered as a function of its proper set of Jacobi [5,15] vectors $\boldsymbol{x}, \boldsymbol{y}, \boldsymbol{z}$ and expanded in angular variables for each coordinate according to

$$\langle \boldsymbol{x}, \boldsymbol{y}, \boldsymbol{z} | F \rangle = \sum_\alpha \frac{F_\alpha(x, y, z)}{xyz} Y_\alpha(\hat{\boldsymbol{x}}, \hat{\boldsymbol{y}}, \hat{\boldsymbol{z}}). \quad (13)$$

The quantities F_α are called regularized FY amplitudes and Y_α are tripolar harmonics, containing spin, isospin, and angular-momentum variables. The label α holds for the set of 10 intermediate quantum numbers describing a $J^\pi, T = 1$ state in the partial-wave basis.

The FY components $F = (K, H)$ are subject to Dirichlet-type boundary condition imposed on a three-dimensional rectangular grid. Both components vanish on any of three (x, y, z) axes, as well as at the borders $x = x_{\max}$ and $y = y_{\max}$ of the chosen resolution grid. On contrary, a boundary condition equivalent to Eq. (9) is imposed on the $z = z_{\max}$ border for the FY components of type K; if no 2+2 particle channels are open, then the FY component of type H must also vanish at the $z = z_{\max}$.

As discussed in the previous section, the expansion of the scattering wave function in terms of the partial-wave basis is, in principle, infinite and a truncation scheme is necessary. In this work the partial-wave basis was truncated to include all the states with $j_x \leqslant 4$, $j_y \leqslant 4$ and $j_z \leqslant 3$, in the so-called j-j coupling scheme [5,15]. By studying the convergence of the calculated phase shifts with respect to the size of the partial-wave basis, we have concluded that this truncation scheme should provide results accurate at 1% level.

The numerical implementation of these equations is described in detail in Ref. [15].

III. RESULTS

In this section we present the phase shifts for the most relevant waves calculated using the three different methods described above. The selected energies for n-^{3}H are $E_n = 1$, 2, 3.5 and 6 MeV, whereas for p-^{3}He they are $E_p = 2.25, 4.05$, and 5.54 MeV, corresponding to cases where experiments have been carried out.

The states considered are those with $J^\pi = 0^\pm$, $1^\pm$, and 2^-. The scattering in other J^π states is dominated by the centrifugal barrier and, therefore, the phase shifts are smaller and not very sensitive to the interaction and the method used to calculate them. Note that, for the $J^\pi = 2^-$ state, we have chosen to report only the $^3P_2$ phase shift, since the $^3F_2$ phase shift and the relative mixing parameter are, in any case, very small. Nevertheless, the coupling between the $^3P_2$ and $^3F_2$ waves has been included in the calculations, since the presence of the $^3F_2$ component in the asymptotic part of the wave function has a sizable effect on the $^3P_2$ phase shift.

Let us remember that the S matrix for elastic n-^{3}H and p-^{3}He scattering has dimension 1 for $J^\pi = 0^\pm$ states and dimension 2 for $J > 0$. In the first case, the S matrix is parametrized, as usual, as $\mathcal{S}^{J\pi}_{LS,LS} = \exp(2i\delta^{J\pi}_{LS})$. For $J > 0$,

TABLE I. n-^{3}H phase shifts and mixing parameters (in degrees) and total cross section σ_t (in barns) for the I-N3LO potential at $E_n = 1.0$, 2.0, 3.5, and 6.0 MeV.

E_n	$^1S_0$	$^3P_0$	$^3S_1$	$^3D_1$	ϵ^{1+}	$^1P_1$	$^3P_1$	ϵ^{1-}	$^3P_2$	σ_t	
1.0	−38.10	4.15	−33.32	−0.09	−0.23	5.99	9.63	9.44	8.98	1.77	AGS
	−38.02	4.10	−33.31	−0.08	−0.22	5.86	9.64	9.14	8.95	1.77	HH
	−38.31	4.00	−33.56	−0.11	−0.24	6.13	10.13	9.6	9.16	1.81	FY
2.0	−51.93	10.54	−45.66	−0.36	−0.44	13.13	24.18	9.15	23.96	2.13	AGS
	−51.98	10.50	−45.72	−0.35	−0.43	13.12	24.25	9.18	23.96	2.13	HH
	−52.34	10.54	−45.99	−0.39	−0.50	13.55	25.15	9.62	24.52	2.19	FY
3.5	−65.54	20.31	−57.99	−0.91	−0.72	20.74	40.94	9.45	43.98	2.38	AGS
	−65.66	20.26	−58.08	−0.91	−0.72	20.94	40.97	9.55	43.91	2.38	HH
	−66.15	20.62	−58.40	−0.91	−0.79	21.17	41.50	9.33	44.42	2.41	FY
6.0	−80.53	32.71	−71.75	−1.77	−1.16	26.88	52.35	10.62	60.04	1.97	AGS
	−80.57	32.55	−71.79	−1.80	−1.15	26.92	52.25	10.68	60.01	1.97	HH
	−80.98	33.40	−71.93	−1.81	−1.22	27.05	52.00	10.71	59.96	1.97	FY

since the S matrix is unitary and symmetric, we can write it as

$$S = O^T S_D O, \tag{14}$$

with S_D a diagonal matrix written as

$$(S_D)_{LS,L'S'} = \delta_{LL'}\delta_{SS'} e^{2i\delta_{LS}^{J\pi}}, \tag{15}$$

where $\delta_{LS}^{J\pi}$ is the phase shift (in the Blatt-Biederharn representation) of the wave LS. Due to the unitarity properties, $\delta_{LS}^{J\pi}$ is a real number. The matrix O in Eq. (14) is parametrized as

$$O = \begin{bmatrix} \cos\epsilon^{J\pi} & \sin\epsilon^{J\pi} \\ -\sin\epsilon^{J\pi} & \cos\epsilon^{J\pi} \end{bmatrix}, \tag{16}$$

TABLE II. Same as in Table I but for the AV18 potential.

E_n	$^1S_0$	$^3P_0$	$^3S_1$	$^3D_1$	ϵ^{1+}	$^1P_1$	$^3P_1$	ϵ^{1-}	$^3P_2$	σ_t	
1.0	−38.52	4.36	−33.67	−0.10	−0.24	6.15	9.64	9.38	8.94	1.80	AGS
	−38.44	4.26	−33.57	−0.09	−0.21	5.87	9.44	9.19	8.82	1.78	HH
	−38.55	4.36	−33.75	−0.09	−0.28	6.14	9.62	9.45	8.93	1.81	FY
2.0	−52.43	10.93	−46.08	−0.38	−0.46	13.30	23.90	8.99	23.45	2.12	AGS
	−52.41	10.82	−46.04	−0.37	−0.42	13.00	23.39	9.19	23.21	2.10	HH
	−52.55	10.92	−46.23	−0.37	−0.47	13.36	23.86	9.07	23.44	2.13	FY
3.5	−66.12	20.75	−58.48	−0.93	−0.75	20.73	40.09	9.24	42.51	2.33	AGS
	−66.14	20.61	−58.53	−0.95	−0.72	20.68	39.63	9.48	42.22	2.32	HH
	−66.23	20.62	−58.66	−0.94	−0.77	20.75	39.98	9.31	42.37	2.33	FY
6.0	−81.03	32.77	−72.19	−1.78	−1.22	26.53	51.13	10.37	57.87	1.93	AGS
	−81.05	32.61	−72.40	−1.87	−1.20	26.55	51.27	10.57	57.94	1.93	HH
	−80.95	32.53	−72.22	−1.86	−1.24	26.58	50.95	10.47	57.57	1.92	FY

TABLE III. Same as in Table I but for the low-k potential derived from the CD Bonn potential. In this case, only the AGS and HH results are reported.

E_n	$^1S_0$	$^3P_0$	$^3S_1$	$^3D_1$	ϵ^{1+}	$^1P_1$	$^3P_1$	ϵ^{1-}	$^3P_2$	σ_t	
1.0	−36.39	3.52	−32.03	−0.08	−0.19	5.34	8.86	9.79	8.37	1.62	AGS
	−36.08	3.41	−31.88	−0.06	−0.19	5.01	8.70	9.34	8.23	1.60	HH
2.0	−49.73	9.03	−43.99	−0.32	−0.37	12.05	22.61	9.76	22.79	1.96	AGS
	−49.61	8.94	−43.95	−0.28	−0.37	11.83	22.51	9.69	22.71	1.95	HH
3.5	−62.94	17.75	−56.01	−0.82	−0.63	19.72	39.30	10.24	43.20	2.26	AGS
	−63.06	17.74	−56.10	−0.79	−0.63	19.88	39.41	10.32	43.25	2.27	HH
6.0	−77.57	29.44	−69.51	−1.66	−1.03	26.38	51.44	11.57	60.41	1.94	AGS
	−77.77	29.46	−69.64	−1.70	−1.04	26.56	51.48	11.63	60.45	1.94	HH

TABLE IV. p-^{3}He phase shifts and mixing parameters (in degrees) for the I-N3LO potential at $E_p = 2.25$, 4.05, and 5.54 MeV.

E_p	$^1S_0$	$^3P_0$	$^3S_1$	$^3D_1$	ϵ^{1+}	$^1P_1$	$^3P_1$	ϵ^{1-}	$^3P_2$	
2.25	−40.64	8.04	−35.00	−0.24	−0.53	10.64	17.29	8.61	16.26	AGS
	−41.23	7.73	−35.47	−0.34	−0.54	10.42	17.11	8.69	16.11	HH
	−41.57	7.74	−35.49	−0.28	−0.58	10.84	17.75	8.43	16.41	FY
4.05	−58.23	17.94	−50.79	−0.94	−0.84	18.90	35.50	8.73	36.61	AGS
	−58.61	17.76	−51.01	−0.97	−0.82	18.97	35.43	8.85	36.53	HH
	−59.12	18.12	−51.15	−0.96	−0.94	19.26	35.78	8.62	36.88	FY
5.54	−68.28	25.41	−60.02	−1.45	−1.08	23.05	44.54	9.28	48.53	AGS
	−68.50	25.07	−60.11	−1.51	−1.07	23.00	44.34	9.36	48.29	HH
	−69.00	25.81	−60.03	−1.40	−1.18	23.16	44.13	9.28	48.33	FY

where $\epsilon^{J\pi}$ is the so-called mixing parameter of the given J^π state. Clearly, the values of the phase shifts and mixing parameters may depend on the (arbitrary) choice on the coupling scheme between the spin of the two clusters and the spherical harmonic function $Y_L(\mathbf{y})$ in the asymptotic functions $\Omega^{\pm}_{LS}$ [see, for example, Eq. (7)]. It can be shown that the phase shifts defined as discussed above are independent on such choices, while the mixing parameter, on the contrary, depends on them. Nevertheless, it is easy to establish the linear relation to transform the mixing parameter from one coupling scheme to another. In the following, we chose to report the mixing parameters defined in the LS coupling scheme by Eq. (7). Moreover, in the following tables, the values reported in a column labeled as $^{2S+1}L_J$ (using the "spectroscopic notation") are relative to the phase shift $\delta^{J\pi}_{LS}$.

In Table I we present the phase shifts, mixing parameters, and total cross sections for n-^{3}H scattering obtained using the I-N3LO potential at the selected energies. By inspecting the table, we can notice the good agreement among the three different techniques. The maximal deviation of the results is less than 1%, fully in line with the estimated errors. Furthermore, the agreement between the results of AGS and HH techniques is even better; in only in a few cases the HH and AGS results differ by more than 0.5%. The strongest deviation, of the order of 0.4°, is observed with the FY results at the largest studied energy. This slightly larger deviation might be due to the necessity by the FY method to perform the transformation of the aforementioned potential to configuration space. In this respect, we note that the AGS calculation is fully performed in momentum space, while in the HH calculation, part of the needed matrix elements are calculated in momentum space (those involving Ψ_C^{LS,JJ_z}, which have to be calculated with more accuracy) and part in configuration space (those involving Ψ_A^{LS,JJ_z}).

In Table II we present the same n-^{3}H results obtained using the AV18 potential. In this case, the convergence of the HH expansion is more problematic, in particular, due to the necessity to extrapolate the HH results. We observe that we still have a very good agreement for the $^1S_0$, $^3P_0$, $^3P_2$, and 1^+ phase shifts, while the differences in the 1^- phase shifts appear to be more enhanced.

In Table III we have reported the phase shifts obtained with the low-k potential derived from CD-Bonn. In this case, the calculations has been performed using the AGS and HH methods, only. We again observe an overall good agreement between the results obtained by the two techniques, except for the lowest energy where the differences are sizable.

The total cross sections σ_t are found to be in agreement within 0.05 b at all considered energies. By comparing the values obtained using the different potentials, we can observe the following well-known characteristics: (i) at low energies the I-N3LO and AV18 models overpredicts the experimental cross section. For example, at $E_n = 1$ MeV, $\sigma_t^{\rm expt} \approx 1.6$ b [27], while $\sigma_t^{\rm I-N3LO} \approx \sigma_t^{\rm AV18} \approx 1.8$ b. On the contrary, with the low-k potential the calculated σ_t is quite close to the experimental one. This behavior is related to the strict relation between the total cross section at low energy and the triton binding

TABLE V. Same as in Table IV but for the AV18 potential.

E_p	$^1S_0$	$^3P_0$	$^3S_1$	$^3D_1$	ϵ^{1+}	$^1P_1$	$^3P_1$	ϵ^{1-}	$^3P_2$	
2.25	−41.11	8.46	−35.26	−0.26	−0.56	10.93	17.35	8.43	16.29	AGS
	−41.53	7.84	−35.65	−0.34	−0.48	10.33	16.76	8.56	15.76	HH
	−41.70	7.82	−36.01	−0.29	−0.52	10.52	17.08	9.01	15.90	FY
4.05	−58.70	18.41	−51.17	−0.93	−0.87	18.89	34.83	8.46	35.65	AGS
	−58.93	17.89	−51.34	−0.98	−0.82	18.85	33.49	8.79	35.33	HH
	−59.02	17.61	−51.76	−1.00	−0.82	18.57	34.81	8.82	35.36	FY
5.54	−68.75	25.82	−60.41	−1.43	−1.12	22.91	43.65	9.00	47.09	AGS
	−68.96	25.05	−60.78	−1.55	−1.10	22.89	43.20	9.32	46.72	HH
	−68.92	24.74	−60.91	−1.55	−1.06	21.93	44.01	8.08	46.53	FY

TABLE VI. Same as in Table IV but for the low-k potential. In this table, only the AGS and HH results are reported. The phase shifts and mixing parameters obtained by the recent PSA [35] are also shown.

E_p	$^1S_0$	$^3P_0$	$^3S_1$	$^3D_1$	ϵ^{1+}	$^1P_1$	$^3P_1$	ϵ^{1-}	$^3P_2$	
2.25	−38.74	6.85	−33.60	−0.21	−0.46	9.63	15.95	9.13	15.13	AGS
	−38.96	6.53	−33.80	−0.26	−0.43	9.21	15.76	8.98	14.91	HH
	−39.1±1.7	5 ± 6	−34.5±0.7			8±2	17±4	10±20	16.5±0.7	PSA
4.05	−55.74	15.60	−48.93	−0.87	−0.75	17.79	34.64	9.43	35.19	AGS
	−56.09	15.48	−49.15	−0.85	−0.74	18.02	33.93	9.54	35.33	HH
	−56.3±0.6	14.1±0.9	−49.3±0.5			17.3±1.6	34.9±0.3	13±2	37.6±0.6	PSA
5.54	−65.54	22.54	−57.97	−1.36	−0.98	22.30	43.13	10.08	47.78	AGS
	−65.97	22.57	−58.18	−1.39	−0.97	22.49	43.21	10.13	47.73	HH
	−67.8±0.9	21.3±0.7	−58.6±0.3			21.2±1.7	45.2±0.5	14±2	51.5±0.5	PSA

energy [14,20,23,28]. (ii) At the peak (around $E_n = 3.5$ MeV), the experimental cross section has been measured to be $\sigma_t^{\rm expt} \approx 2.45$ b [27]. In this case we note that the AV18 and low-k potential models underpredict sizeably the experimental value, while $\sigma_t^{\rm I-N3LO}$ is quite close to it.

Let us now consider p-^{3}He scattering. The phase shifts and mixing parameters obtained within the three methods have been reported in Tables IV, V, and VI, corresponding respectively to the I-N3LO, AV18, and low-k NN potential models. Here the differences between the various techniques are larger than in the n-^{3}H case, especially at low energy and for the $J^\pi = 0^\pm$ states. For the AV18 potential, we note that the HH results are more or less intermediate between the AGS and FY results.

In Table VI we have also reported the phase shifts and mixing parameters obtained by the recent PSA [35]. Note that the low-k potential used in this work is the only potential which does not underestimate the ^{4}He binding energy. The PSA estimates have rather large errors. However, it is possible to draw some conclusions about the capability of this low-k potential model to describe the experimental data. As can be seen, the PSA S-wave phase shifts seem to be well reproduced (except for the $^1S_0$ phase shift at 5.54 MeV) by the calculations. Also the $^3P_0$ and $^1P_1$ agree well, but for these cases the experimental errors are large. On the other hand, we note a sizable underestimation of the large $^3P_1$ and $^3P_2$ phase shifts.

Let us now see how the fairly good agreement found for the phase shifts and mixing parameters calculated with the three different methods reflects on the observables. We have considered the differential cross section and the neutron (proton) analyzing power A_{y0} for n-^{3}H (p-^{3}He) elastic scattering at the considered energies, as functions of the center-of-mass scattering angle. Furthermore, we have also considered the triton (^{3}He) analyzing power A_{0y}. This observable is, in fact, rather sensitive to small variations of the phase shifts in the kinematical regime considered in this article.

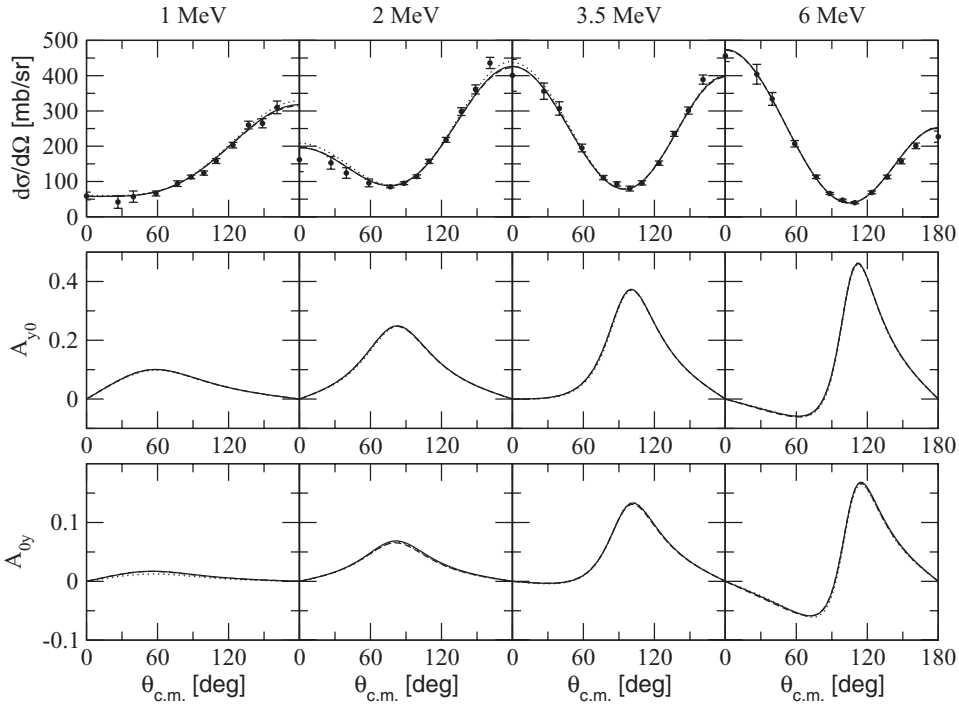

FIG. 1. Differential cross section and neutron and triton analyzing powers A_{y0} and A_{0y} for n-^{3}H elastic scattering at $E_n = 1, 2, 3.5$, and 6 MeV neutron laboratory energies as functions of the center-of-mass scattering angle. Results obtained using the AGS equation (solid lines), the HH expansion method (dashed lines), and the FY equations (dotted lines) using the I-N3LO potential are compared. For most of the cases the three curves coincide and cannot be distinguished. The experimental data are from Ref. [46].

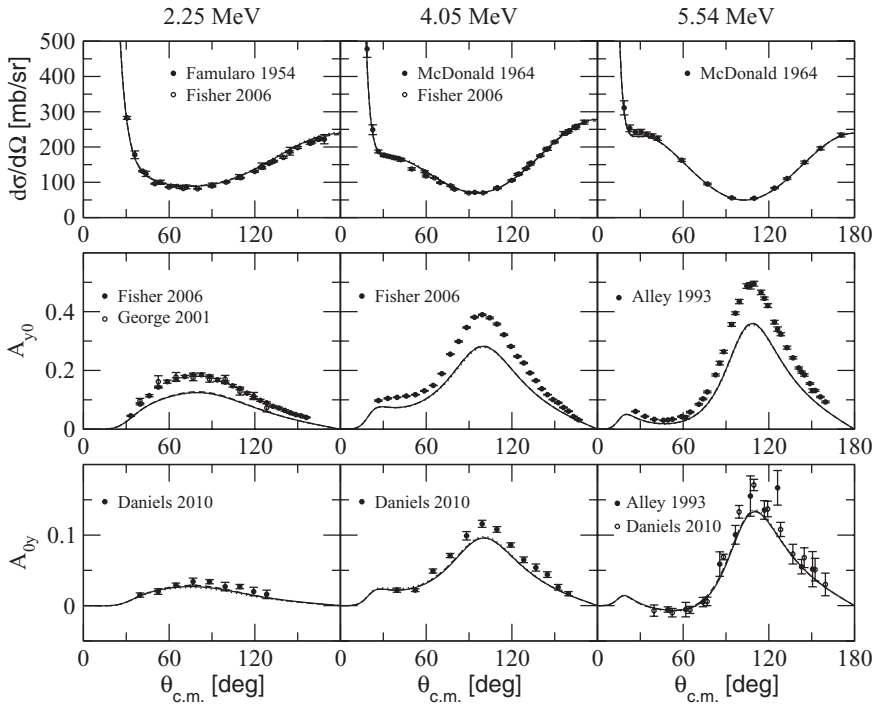

FIG. 2. Same as in Fig. 1 but for p-^{3}He elastic scattering at $E_p = 2.25$, 4.05, and 5.54 MeV proton laboratory energies. The experimental data are from Refs. [29–33,35].

In Figs. 1 and 2 we have reported the results obtained using the AGS equation (solid lines), the HH expansion method (dashed lines), and the FY equations (dotted lines) using the I-N3LO potential. As can be seen by inspecting the two figures, the three curves almost always perfectly coincide and cannot be distinguished. We have also reported the experimental data for the n-^{3}H differential cross section [46] and the three p-^{3}He observables [29–33,35]. We note that the differences between the three calculations, where they can be appreciated, are in any case always smaller than the experimental errors.

The agreement between the three calculations when the AV18 potential is adopted is again rather satisfactory, as can be seen in Figs. 3 and 4. A small disagreement can be observed only for the A_{0y} observable (see the panels in the last row of Fig. 4). This observable is also rather sensitive to the small D-wave and F-wave phase shifts not reported in Tables II and V. We already know that the AV18 model contains a stronger repulsion than the I-N3LO at short interparticle distances. As discussed above, the convergence of the HH method for this case is more problematic and, consequently, the calculations

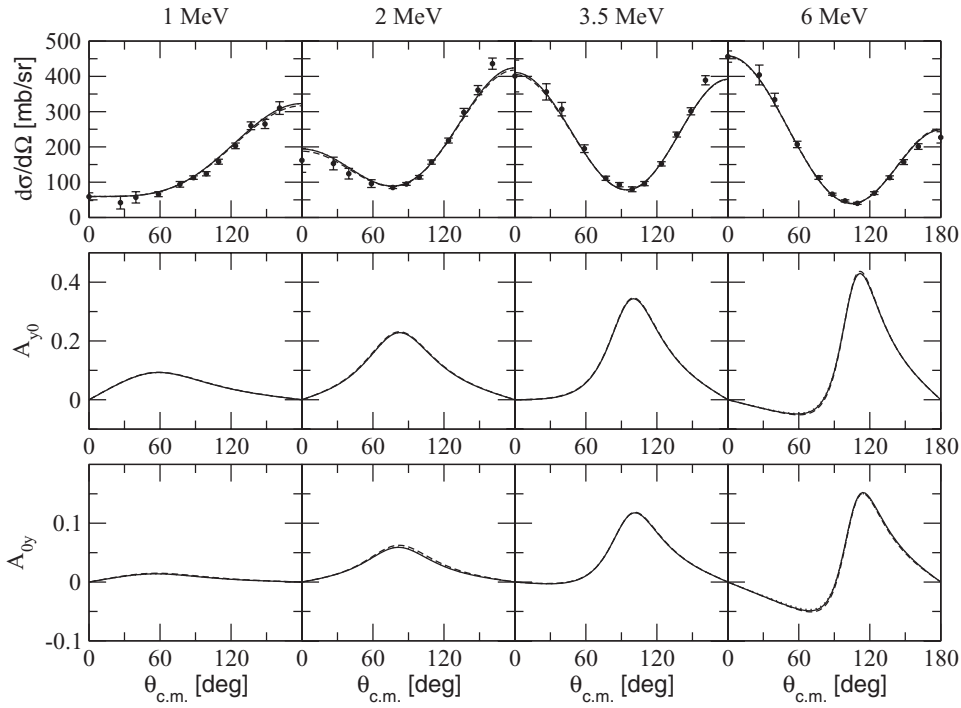

FIG. 3. Same as in Fig. 1 but for the AV18 potential.

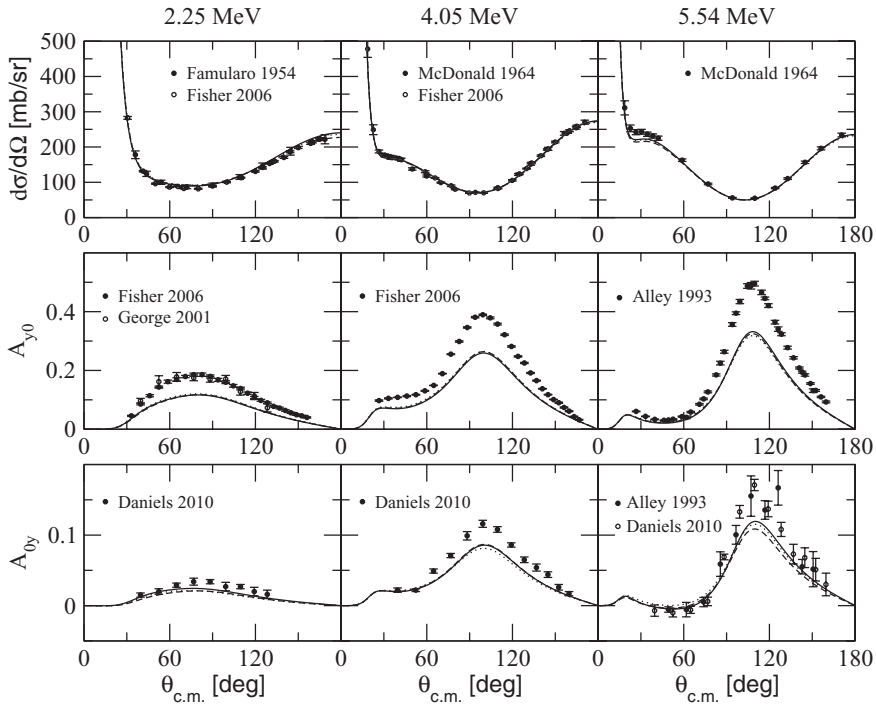

FIG. 4. Same as in Fig. 2 but for the AV18 potential.

have a larger uncertainty. In spite of these difficulties, the agreement in the considered observables is still quite good.

Let us consider now the low-k potential, which has no repulsion at short interparticle distance. Consequently, in this case, we expect a good agreement between the results of the different techniques. For this potential, the calculations have been performed using the AGS (solid curves) and HH (dashed curves) methods only, and the corresponding results are reported in Figs. 5 and 6. The two curves are practically indistinguishable, confirming that for soft potentials the convergence of the calculations is excellent.

Finally, in the literature for p-^{3}He scattering, there exist measurements of other spin-correlation observables (A_{yy}, A_{xx}, A_{zz}, A_{xz}, and A_{zx}). Also for these observables we have found a good agreement between the predictions obtained by the three different methods, for all the potential models considered here. The comparison of the theoretical predictions and the experimental data for these observables will be discussed in the next section.

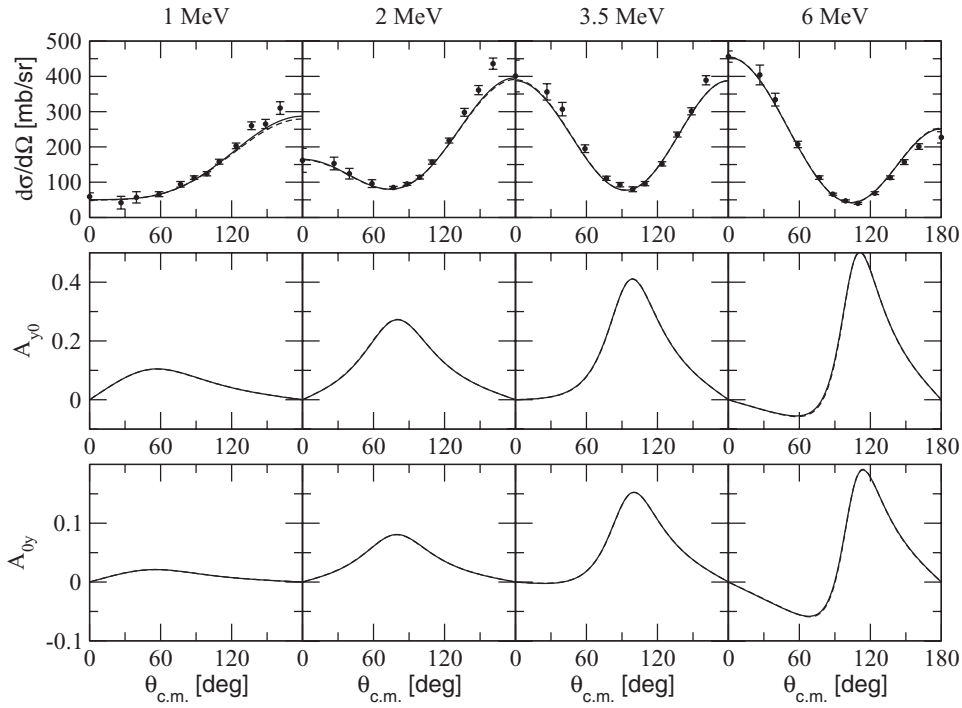

FIG. 5. Same as in Fig. 1 but for the low-k potential. Only the AGS and HH results are reported.

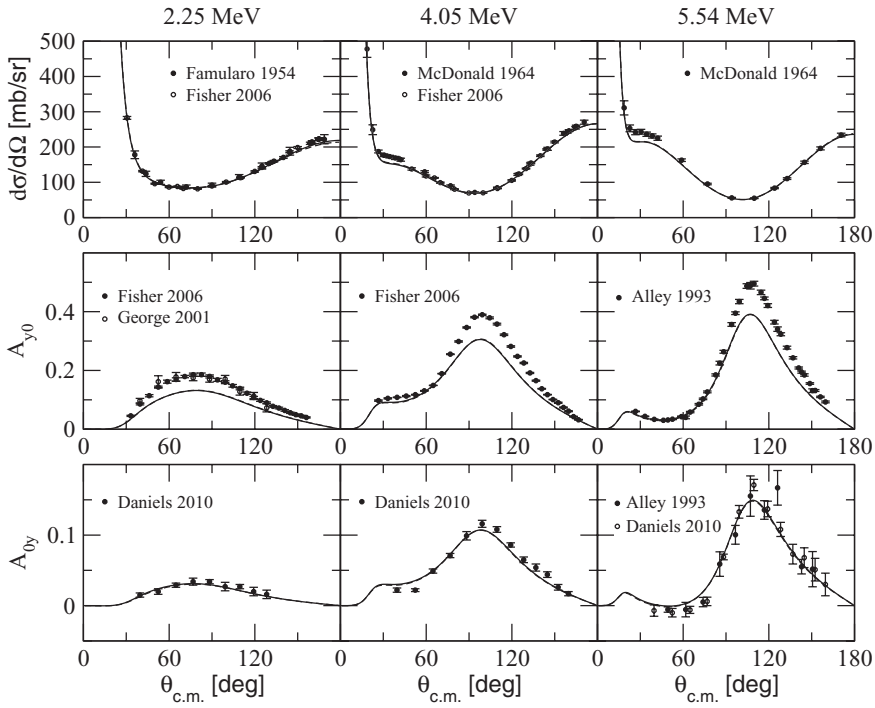

FIG. 6. Same as in Fig. 2 but for the low-k potential. Only the AGS and HH results are reported.

IV. COMPARISON WITH EXPERIMENTAL DATA

In this section we discuss the comparison between the theoretical calculations and the experimental data. We consider here only p-^{3}He scattering since for this process the experimental data are more abundant and precise. The figures presented in this section can be considered an update of

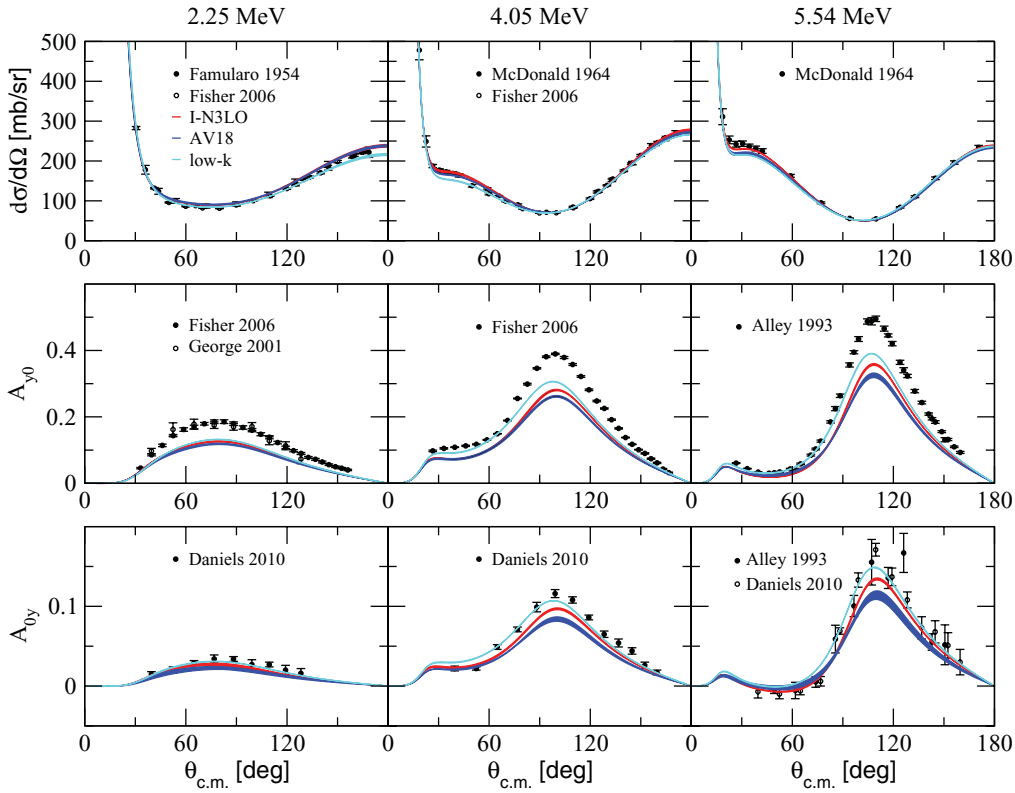

FIG. 7. (Color online) Differential cross section, proton analyzing power, and ^{3}He analyzing power for p-^{3}He elastic scattering at $E_p = 2.25$, 4.05, and 5.54 MeV proton laboratory energies obtained using the I-N3LO (red bands), AV18 (blue bands), and the low-k (cyan bands) potential models. The experimental data are from Refs. [29–33,35].

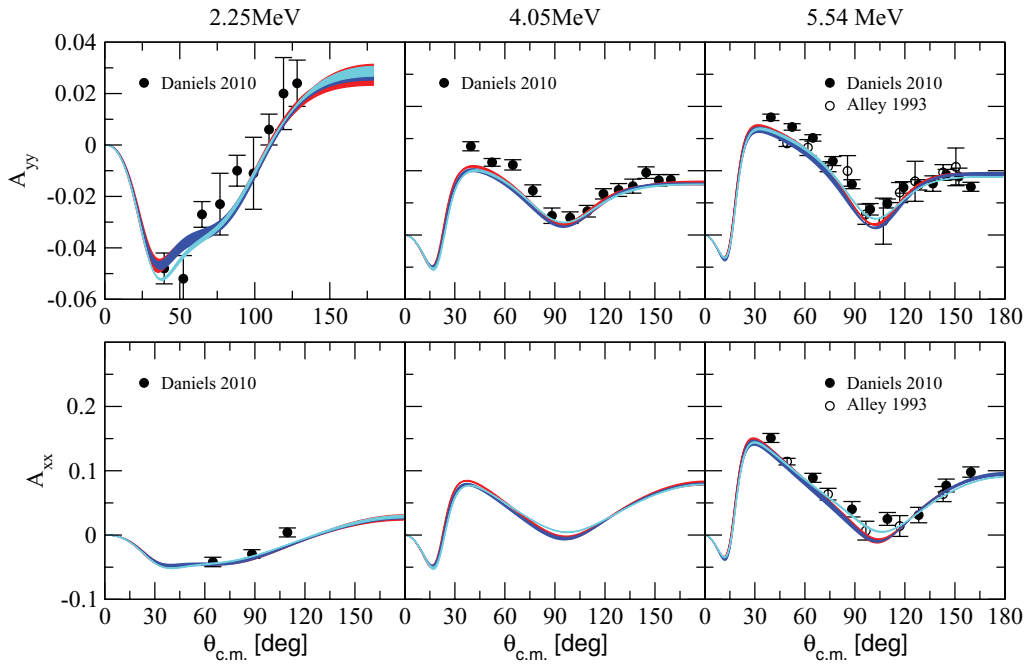

FIG. 8. (Color online) Same as in Fig. 7 but for the spin-correlation A_{yy} and A_{xx} observables. The experimental data are from Refs. [32,35].

previous comparisons [7,8,17,21,31]. For the three observables considered so far ($d\sigma/d\Omega$, A_{y0}, and A_{0y}), the comparison between theory and experiment can be inferred already from Figs. 1–6. However, in order to better appreciate the differences in the predictions obtained by the three potential models as compared to the experimental data, we summarize again in Fig. 7 the results for $d\sigma/d\Omega$, A_{y0}, and A_{0y}. In order to take into account the (slight) different predictions obtained using the three different theoretical methods, we have decided to present the calculated observables for each potential as bands. Each band contains the results obtained by using the three different methods. As can be seen from Fig. 7, the differential unpolarized cross sections obtained using the I-N3LO potential (red bands) agree well with the experimental data. With the other two potentials we observe some disagreement, in particular around $\theta_{\text{c.m.}} \approx 30^\circ$ and in the large scattering angle region. The results obtained for A_{y0} are found to depend on the potential model. Here, we observe the well-known underprediction of the experimental data by the theoretical calculations. Interestingly, the results obtained with the low-k potential are in a better agreement with the experimental A_{y0}. A similar situation is found also for A_{0y}, as can be seen in the three lower panels of Fig. 7. It is worth noting that the effect of supplementing the AV18 potential with the Urbana 3N force model [47] has been found to be almost negligible for this observable [31]. The inclusion of the new chiral 3N potential derived in Ref. [48] is under study [43] (see Ref. [20] for a preliminary report).

In Fig. 8, we report the results found for the A_{yy} and A_{xx} spin correlations at the three different proton energies. As can be seen, for these two observables the predictions obtained with the three potentials are almost identical. We observe that the calculated A_{yy} is slightly at variance with respect to the experimental data, while the A_{xx} observable is reasonably well reproduced by the calculations.

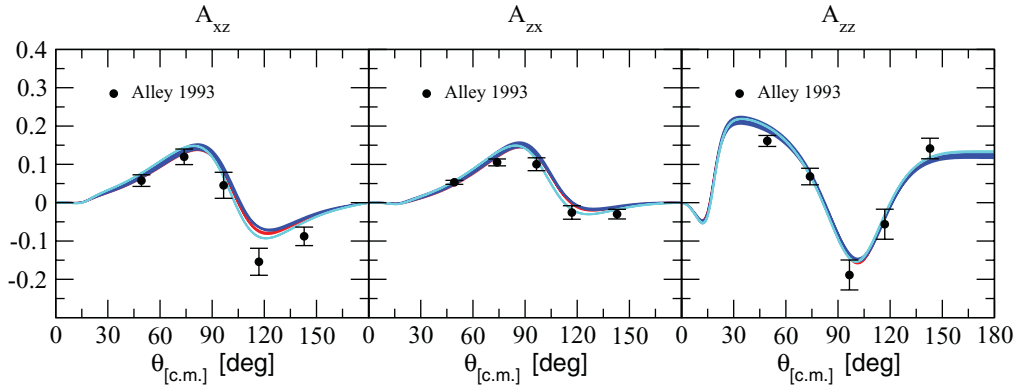

FIG. 9. (Color online) Same as in Fig. 7 but for the spin-correlation A_{xz}, A_{zx}, and A_{zz} observables (at $E_p = 5.54$ MeV proton laboratory energy only). The experimental data are from Ref. [32].

Finally, in Fig. 9 we compare the results obtained for the A_{xz}, A_{zx}, and A_{zz} spin-correlation observables. In this case, only the $E_p = 5.54$ MeV proton laboratory energy is considered, since only for this energy experimental data exist. Also in this case, the sensitivity to the different potential models is not significant. Moreover, the calculations reproduce well the (few) experimental data.

V. CONCLUSIONS

In this work, we have studied several low-energy n-^{3}H and p-^{3}He elastic observables by use of three different approaches, the HH, AGS, and FY techniques. In 2007, some of the authors of the present paper presented very accurate solutions of the four-nucleon scattering problem using the AGS technique [7–9]. They were able to take into account the long-range Coulomb interaction using the screening-renormalization method [12,13]. In recent years, also the accuracy of the calculations performed using the HH and FY techniques increased [18,20,21]. Therefore, it becomes appropriate to compare the results obtained by the different methods in order to test their capability to solve the $4N$ scattering problem. This is the primary aim of the present article. Another important motivation is to provide a set of solid converged results in the literature, which could represent useful benchmarks for future applications in $A = 4$ scattering.

In the present article we have shown that for I-N3LO and the selected low-k potential model, which have a "soft" repulsion at short interparticle distances (the low-k model has no repulsion at all), the results obtained by use of the different techniques are in very good agreement. With the AV18 potential, the agreement is not so perfect, although the (slight) differences can be appreciated only for some small polarization observables. We can conclude, therefore, that the $A = 4$ scattering problem is nowadays solved with a very good accuracy, better than 1%.

Concerning the comparison with the experimental data, we have confirmed the large underprediction of the p-^{3}He A_{y0} observable, a problem already put in evidence some time ago [14,33,34] and certainly related to the $N - d$ "A_y puzzle." For this observable we have observed a moderate dependence on the considered potential models. The low-k potential is found to give a better description of the observable when compared with the experimental data. However, the same potential does not reproduce well the unpolarized cross section. We have also found a small underprediction of the theoretical A_{0y} and A_{yy} observables, while other measured observables, such as A_{xx}, A_{xz}, A_{zx}, and A_{zz} spin-correlation coefficients, show less sensitivity to the potential models. They are in good agreement with the available (sparse) experimental data.

The discrepancies found, in particular, for A_{y0}, indicate serious limitations of the existing NN force models to describe the $4N$ continuum. These difficulties can hardly be solved by the inclusion of a standard type 3N force, used to reproduce the few-nucleon binding energies [17,21,31]. Instead, its origin could lie either in the NN forces themselves or in the presence of a 3N force of unknown type. Clearly, an eventual solution of the $A = 4$ A_{y0} problem should be related in some way to the solution of the $N - d$ "A_y puzzle."

Finally, we conclude by noting that it would be interesting to extend the present analysis to p-^{3}H, n-^{3}He, and d-d scattering observables, which have already been calculated in the framework of the AGS equations for different NN interactions [9,10].

ACKNOWLEDGMENTS

The FY work was performed using the HPC resources of IDRIS under the allocation 2010-i2009056006 made by GENCI (Grand Equipement National de Calcul Intensif). We thank the staff members of the IDRIS for their constant help.

[1] H. Kamada *et al.*, Phys. Rev. C **64**, 044001 (2001).
[2] B. S. Pudliner *et al.*, Phys. Rev. C **56**, 1720 (1997).
[3] R. B. Wiringa *et al.*, Phys. Rev. C **62**, 014001 (2000).
[4] A. Nogga *et al.*, Phys. Rev. C **65**, 054003 (2002).
[5] R. Lazauskas and J. Carbonell, Phys. Rev. C **70**, 044002 (2004).
[6] M. Viviani, A. Kievsky, and S. Rosati, Phys. Rev. C **71**, 024006 (2005); D. Gazit *et al.*, Phys. Rev. Lett. **96**, 112301 (2006).
[7] A. Deltuva and A. C. Fonseca, Phys. Rev. C **75**, 014005 (2007).
[8] A. Deltuva and A. C. Fonseca, Phys. Rev. Lett. **98**, 162502 (2007).
[9] A. Deltuva and A. C. Fonseca, Phys. Rev. C **76**, 021001 (2007).
[10] A. Deltuva and A. C. Fonseca, Phys. Rev. C **81**, 054002 (2010).
[11] A. Deltuva, A. C. Fonseca, and P. U. Sauer, Phys. Lett. B **660**, 471 (2008).
[12] E. O. Alt, W. Sandhas, and H. Ziegelmann, Phys. Rev. C **17**, 1981 (1978); E. O. Alt and W. Sandhas, *ibid.* **21**, 1733 (1980).
[13] A. Deltuva, A. C. Fonseca, and P. U. Sauer, Phys. Rev. C **72**, 054004 (2005); Phys. Rev. Lett. **95**, 092301 (2005).
[14] F. Ciesielski, Ph.D Thesis, Thèse Univ. J. Fourier (Grenoble), 1997; F. Cieselski and J. Carbonell, Phys. Rev. C **58**, 58 (1998); F. Ciesielski, J. Carbonell, and C. Gignoux, Phys. Lett. B **447**, 199 (1999).
[15] R. Lazauskas, Ph.D Thesis, Thèse Univ. J. Fourier (Grenoble), 2003.
[16] R. Lazauskas and J. Carbonell, Nucl. Phys. A **737**, S79 (2004).
[17] R. Lazauskas *et al.*, Phys. Rev. C **71**, 034004 (2005).
[18] R. Lazauskas, Phys. Rev. C **79**, 054007 (2009).
[19] A. Kievsky *et al.*, J. Phys. G: Nucl. Part. Phys. **35**, 063101 (2008).
[20] M. Viviani *et al.*, Few-Body Syst. **45**, 119 (2009).
[21] M. Viviani *et al.*, EPJ Web of Conferences **3**, 05011 (2010).
[22] H. M. Hofmann and G. M. Hale, Nucl. Phys. A **613**, 69 (1997).
[23] B. Pfitzinger, H. M. Hofmann, and G. M. Hale, Phys. Rev. C **64**, 044003 (2001).
[24] H. M. Hofmann and G. M. Hale, Phys. Rev. C **68**, 021002 (2003); **77**, 044002 (2008).
[25] S. Quaglioni and P. Navrátil, Phys. Rev. Lett. **101**, 092501 (2008).
[26] R. Wiringa (unpublished).

[27] T. W. Phillips, B. L. Berman, and J. D. Seagrave, Phys. Rev. C **22**, 384 (1980).
[28] M. Viviani, S. Rosati, and A. Kievsky, Phys. Rev. Lett. **81**, 1580 (1998).
[29] K. F. Famularo *et al.*, Phys. Rev. **93**, 928 (1954).
[30] D. G. McDonald, W. Haberli, and L. W. Morrow, Phys. Rev. **133**, B1178 (1964).
[31] B. M. Fisher *et al.*, Phys. Rev. C **74**, 034001 (2006).
[32] M. T. Alley and L. D. Knutson, Phys. Rev. C **48**, 1890 (1993).
[33] M. Viviani *et al.*, Phys. Rev. Lett. **86**, 3739 (2001); E. A. George and L. D. Knutson, Phys. Rev. C **67**, 027001 (2003).
[34] A. C. Fonseca, Phys. Rev. Lett. **83**, 4021 (1999).
[35] V. T. Daniels *et al.*, Phys. Rev. C **82**, 034002 (2010).
[36] D. R. Entem and R. Machleidt, Phys. Rev. C **68**, 041001 (2003).
[37] R. B. Wiringa, V. G. J. Stoks, and R. Schiavilla, Phys. Rev. C **51**, 38 (1995).
[38] S. K. Bogner, T. T. S. Kuo, and A. Schwenk, Phys. Rep. **386**, 1 (2003).
[39] R. Machleidt, Phys. Rev. C **63**, 024001 (2001).
[40] P. Grassberger and W. Sandhas, Nucl. Phys. B **2**, 181 (1967); E. O. Alt, P. Grassberger, and W. Sandhas, JINR Report No. E4-6688 (1972).
[41] A. Deltuva, A. C. Fonseca, and P. U. Sauer, Phys. Rev. C **71**, 054005 (2005).
[42] L. E. Marcucci *et al.*, Phys. Rev. C **80**, 034003 (2009).
[43] M. Viviani *et al.*, in preparation.
[44] O. A. Yakubovsky, Sov. J. Nucl. Phys. **5**, 937 (1967).
[45] L. D. Faddeev, Zh. Eksp. Teor. Fiz. **39**, 1459 (1960) [Sov. Phys. JETP **12**, 1014 (1961)].
[46] J. D. Seagrave, L. Cranberg, and J. E. Simmons, Phys. Rev. **119**, 1981 (1960).
[47] B. S. Pudliner *et al.*, Phys. Rev. C **56**, 1720 (1997).
[48] P. Navrátil, Few-Body Syst. **41**, 117 (2007)